Surface Plasmon Resonance Sensor Based on Double-Sided Polished Microstructured Optical Fiber With Hollow Core

Donglian Hou, Xianxing Ji, Nannan Luan, Li Song, Yongsheng Hu, Mingming Luo, Jingfei He, Zhenxu Bai, Zhenao Bai, and Jianfei Liu

***Abstract*—A surface plasmon resonance sensor based on double-sided polished microstructured optical fiber with hollow core is put forward for refractive index sensing. Two gold films parallel to each other attached to the polished surface act as microfluidic sensing channels for the analyte. The artificially introduced air hole can facilitate the phase matching between the core mode and the plasmon mode. The sensitivities of the proposed sensor are investigated by the wavelength, amplitude and phase interrogation methods when the analyte refractive index increases from 1.33 to 1.34. In contrast to the D-shaped design, the double-sided polished structure demonstrates narrower resonance spectral width and greater phase sensitivity. Moreover, the numerical results indicate that the proposed sensor shows a good stability in the fabrication tolerances of $\pm 5\%$ of the thickness of gold film and the depth of polishing, respectively.**

***Index Terms*—Fiber optics sensors, surface plasmon resonance, microstructured optical fiber, refractive index sensors.**

I. Introduction

SURFACE plasmon resonance (SPR) is the excitation of the surface plasmon coupled with the oscillations of free electron density between the metal and dielectric [1]–[5]. By comparison with conventional methods, SPR is an effective sensing technology that is extremely sensitive to changes in surrounding dielectric refractive index (RI), providing characteristics including no marking, real-time detection, high speed and sensitivity. Therefore, it has been applied extensively in bio-sensing, medical diagnostics, drug development, food safety and so on [6]–[22]. Among the various kinds of the SPR sensing configurations, the microstructured optical fiber (MOF) can be immaculately integrated with SPR, owing to its small size, lesser weight, flexible structure, fast response and more practical [20]–[39]. Compared with the other types of SPR sensors, such as prism based SPR and optical fiber based SPR sensors [1]–[19], the main advantage of flexible structure of the MOF is that it can alleviate phase-matching problem between the core mode and the surface plasmon polariton (SPP) mode, and thus improving the sensitivity [20]–[23], [34]–[39]. However, there are two major problems in the MOF-SPR sensors: one is the difficult fabrication of sensor and the other is the broadened spectral width of the resonance peaks. In the process of sensors fabrication, it contains metal coating on the inner wall of the air holes and filling the air holes with the analyte [20]–[39]. It is very sophisticated process in a few micrometer holes from fabrication point of view. On the other hand, to facilitate phase-matching, one has to introduce the air holes in the fiber core to lessen the effective refractive index (n_{eff}) of the core mode [34]–[39]. However, the introduced air holes also create an extra loss in the core modes, which causes a broader resonance spectral width and thus reducing the resolution of the SPR sensors in the wavelength interrogation mode. Although the resonance spectrum width can be decreased by selective coating of metal film in the MOF [37]–[39], the difficulty of making the sensors has been further increased.

Recently, the SPR sensors based on D-shape or side-opening MOFs have obtained extensive attention for their unique structures [40]–[53]. The problems of the metal coating and analyte filling in the micrometer holes can be impeccably avoided by coating the open part of them with the metal film and being in contact with the analyte directly [40]–[53]. Moreover, by introducing the air hole into fiber core area, the D-shape or side-opening MOF structures can also alleviate the phase-matching problem [40], [48]. In brief, the problems of processing complex and phase-matching can be simultaneously alleviated by employing the D-shape or side-opening MOF with hollow

Manuscript received May 17, 2021; revised June 26, 2021; accepted July 12, 2021. Date of publication July 16, 2021; date of current version August 3, 2021. This work was supported in part by the Natural Science Foundation of Hebei Province under Grants F2019202294, F2019202337, A2020202013, F2019202387, and F2019202252, in part by the National Key Research and Development Program of China under Grant 2017YFB1104503, and in part by the Guangdong Key Research and Development Program under Grant 2018B090904003. *(Corresponding author: Nannan Luan.)*

Donglian Hou, Xianxing Ji, Nannan Luan, Li Song, Mingming Luo, and Jingfei He are with the Tianjin Key Laboratory of Electronic Materials and Devices, School of Electronics and Information Engineering, Hebei University of Technology, Tianjin 300401, China (e-mail: 201921902013@stu.hebut.edu.cn; 202021902017@stu.hebut.edu.cn; nannanluan@gmail.com; songli@hebut.edu.cn; 2019013@hebut.edu.cn; hejingfei@hebut.edu.cn).

Yongsheng Hu is with the School of Physics and Microelectronics, Zhengzhou University, Zhengzhou 450001, China (e-mail: h0y0s@163.com).

Zhenxu Bai and Jianfei Liu are with the Tianjin Key Laboratory of Electronic Materials and Devices, School of Electronics and Information Engineering, Hebei University of Technology, Tianjin 300401, China, and also with the Hebei Key Laboratory of Advanced Laser Technology and Equipment, Tianjin 300401, China (e-mail: baizhenxu@hotmail.com; jfliu@hebut.edu.cn).

Zhenao Bai is with the Aerospace Information Research Institute, Chinese Academy of Sciences, Beijing 100094, China (e-mail: baizhenao@hotmail.com).

Digital Object Identifier 10.1109/JPHOT.2021.3097368

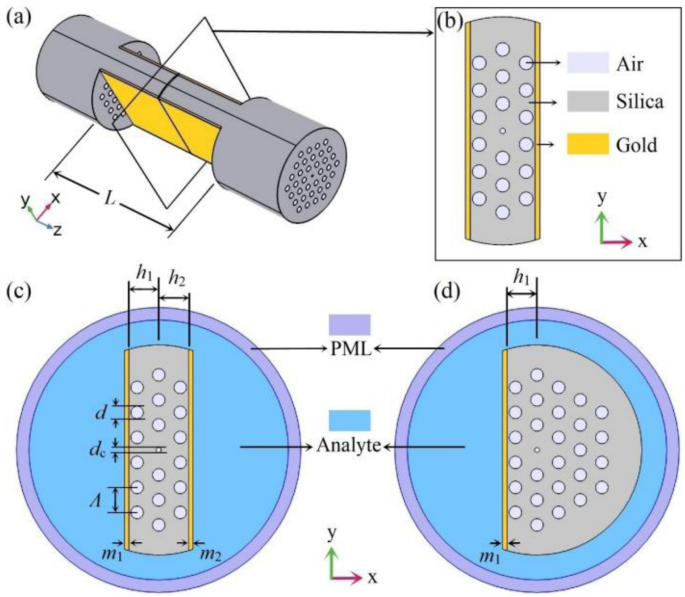

Fig. 1. (a) 3D view of the SPR sensor based on double-sided polished MOF. (b) Cross-sectional view of the proposed SPR sensor. (c) Schematic diagram of the proposed SPR sensor with boundary condition. (d) Schematic diagram of the SPR sensor based on D-shaped MOF with boundary condition.

core. However, the phenomenon of spectral broadening caused by the introducing air hole at fiber core area still remains unsettled [40], [48].

In this paper, we design a new SPR sensor based on double-sided polished MOF with hollow core. Owning to double-sided channels in RI sensing, the advantages of the proposed sensor are that it can not only simplify the fabricating process compared to the inside coating and filling MOF-SPR sensors, but also support narrower spectral width than the D-shaped MOF-SPR sensors. We investigate sensing properties of the proposed sensor, incorporating spectral widths, wavelength, amplitude and phase sensitivities, in comparison with the D-shaped SPR sensor based on MOF with hollow core, and fabrication tolerances with respect to the thickness of gold film and the depth of polishing. The discussion and analyses in this paper allow us to better understand the coupling between the SPP mode and core mode of such sensor and also promote it to be a great candidate in SPR sensing applications.

II. Schematic and Method

The 3D schematic diagram and cross section of the proposed SPR sensor based on double-sided polished MOF with hollow core are shown in Fig. 1(a) and (b), respectively. The cladding of the fiber consists of three layers air holes in regular hexagon around the fiber core to lower its average RI for restricting the transmit of light in the core. Monolayer air holes on the left and right sides of the core are reserved by polishing the fiber into flat plane uniformly. The polished planes are deposited with gold film as a plasmonic material, whose outer surfaces can be flowed through analyte, which simplifies the sensor structure. A smaller air hole is introduced into the fiber core that can facilitate and tune the phase matching between the core mode and the SPP mode significantly.

The electromagnetic mode of the sensor fiber is settled by the commercially available software package COMSOL Multiphasics, with perfect match layer (PML) added to the outmost layer, as shown in Fig. 1(c). The lattice pitch of regular hexagon is $\Lambda = 2$ μm, and the diameters of the cladding air holes and the core air hole are $d = 0.5\Lambda$, $d_c = 0.2\Lambda$, respectively. The polishing depths of h_1 and h_2 are both 1.2Λ, which are the distances from the fiber core to the two polished surfaces respectively. The thicknesses of the gold films are $m_1 = m_2 = 40$ nm. The RI of the silica of the background material (n) is defined as follows by Sellmeier Equation [28]:

$$\mathrm{n}^2(\lambda) = 1 + \frac{\mathrm{B}_1\lambda^2}{\lambda^2 - \mathrm{C}_1} + \frac{\mathrm{B}_2\lambda^2}{\lambda^2 - \mathrm{C}_2} + \frac{\mathrm{B}_3\lambda^2}{\lambda^2 - \mathrm{C}_3} \quad (1)$$

where the λ is the operating wavelength in microns, and B_1, B_2, B_3, C_1, C_2 and C_3 are Sellmeier coefficients whose values are referred to in [28]. The RI of air is assumed to be 1. The permittivity of the gold $\varepsilon(\omega)$ of gold is described as by the Drude-Lorentz model [54]:

$$\varepsilon(\omega) = \varepsilon_\infty - \frac{\omega_D^2}{\omega(\omega + j\gamma_D)} - \frac{\Delta\varepsilon\Omega_L^2}{(\omega^2 - \Omega_L^2) + j\Gamma_L\omega} \quad (2)$$

where ε_∞ is permittivity at high frequency, and ω is the angular frequency of an incident light, $\omega = 2\pi/\lambda$. Moreover, ω_D is the plasma frequency and γ_D is the damping frequency. $\Delta\varepsilon$ is the weighting factor, Ω_L and Γ_L are the spectral width and oscillator strength, respectively. The above parameter values can be read in [54].

For comparison, we also investigate the hollow-core D-shaped MOF based SPR sensor with the same parameters as shown in Fig. 1(d), and compare about the mode characteristics and the sensing performances of the two sensor structures.

III. Numerical Result and Analysis

For the guided light in the fiber core, the evanescent wave propagates along the boundary of the medium. Resonance occurs when the light momentum matches that of the electron oscillation at the metal dielectric interface. At the same time, the intensity of the transmitted light is vastly weakened because of the transferred energy from photon to plasmon. And therefore the degree of resonance is determined through detecting the loss of energy in the core mode [20]–[53]. Based on this principle, we can monitor the energy transfer between the core mode and SPP mode of structure of two sensors. It should be noted that only the *x*-polarized core mode is considered because of the fact that the SPP mode generated by the gold surface can only couple with the *x*-polarized core mode with the same polarization direction [40]–[44]. As shown in Fig. 2, at 500 nm (non-resonance region), for instance, the energy of the light mainly concentrates in the core mode region. And it starts transferring gradually following the growth of wavelength. When the wavelength reaches 583 nm that satisfies the phase-matching condition, the transfer of energy from the *x*-polarized core mode to the SPP mode achieves maximum. There is a markedly difference that the energy of the *x*-polarized core mode of double-sided polished sensor transfers

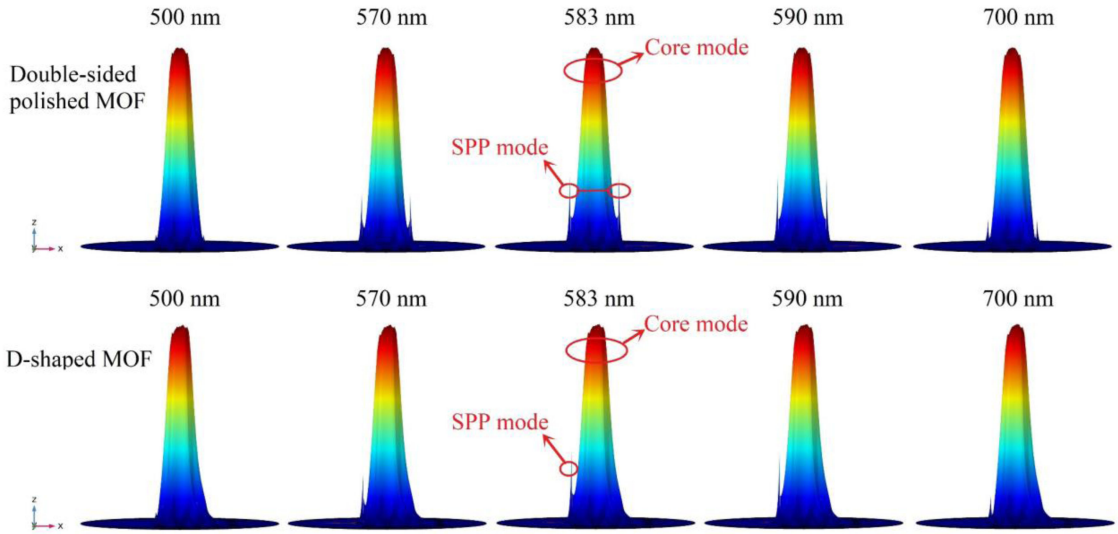

Fig. 2. Energy transfer between the x-polarized core mode and SPP mode of the double-sided polished MOF-SPR sensor and D-shaped MOF-SPR sensor at several different wavelengths.

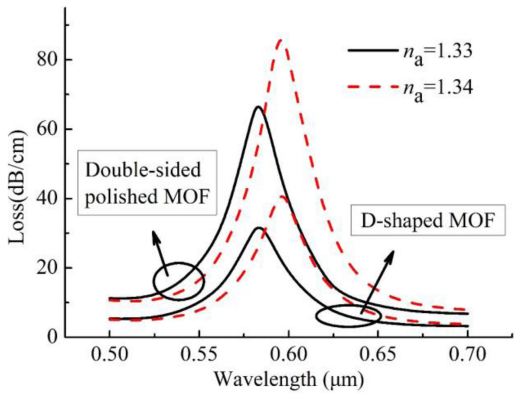

Fig. 3. Loss spectra of the *x*-polarized core mode of the double-sided polished MOF-SPR sensor and D-shaped MOF SPR sensor with n_a at 1.33 and 1.34.

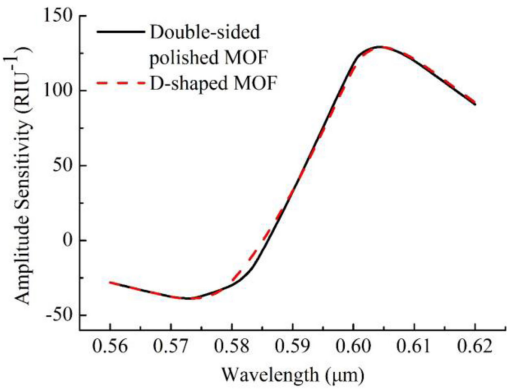

Fig. 4. The amplitude sensitivities of the curves of the double-sided polished MOF-SPR sensor and D-shaped MOF SPR sensor when na changes from 1.33 to 1.34.

to double-sided SPP modes while that of D-shaped sensor transfers to single-sided SPP mode, which means the double-sided polished sensor has more prominent coupling with core mode. Fig. 3 presents loss spectra of the *x*-polarized core mode in the wavelength of range from 500 nm to 700 nm when RI of analyte (n_a) varies from 1.33 to 1.34. For evaluating the sensing performance, there are three main interrogation modes of the proposed sensor detection–wavelength interrogation, amplitude interrogation and phase interrogation modes.

A. *Wavelength Interrogation Mode*

In the wavelength interrogation mode, the change of n_a can be judged by the shift of the wavelength of resonance peak. The wavelength sensitivity is defined as follows [34]

$$S_\lambda\,(nm/RIU) = \frac{\Delta\lambda_{peak}}{\Delta n_a} \tag{3}$$

where $\Delta\lambda_{\rm peak}$ is the shift of resonance peak wavelength and Δn_a is the change of n_a.

For the two sensors, the $\Delta\lambda_{\rm peak}$ are both from 583 nm at $n_a = 1.33$ to 596 nm at $n_a = 1.34$. Therefore, the two structures have the same wavelength sensitivity 1300 nm/RIU calculated according to (3). From the Fig. 3, it is important to note that, compared with the D-shaped structure, the double-sided structure owns greater loss at the resonance peak due to its two gold-coating polished surfaces that generate more SPP modes to couple with the *x*-polarized core mode. As a result, the resonance spectral width becomes narrower, and thus improving the signal to noise ratio (SNR) [38].

B. *Amplitude Interrogation Mode*

The amplitude interrogation mode, characterized by the simpler detection without spectral involvement, is performed at a certain wavelength. The amplitude sensitivity is given by [34]

$$S_A\left(RIU^{-1}\right) = \frac{1}{\alpha\left(\lambda, n_a\right)} \cdot \frac{\Delta\alpha\left(\lambda, n_a\right)}{\Delta n_a} \tag{4}$$

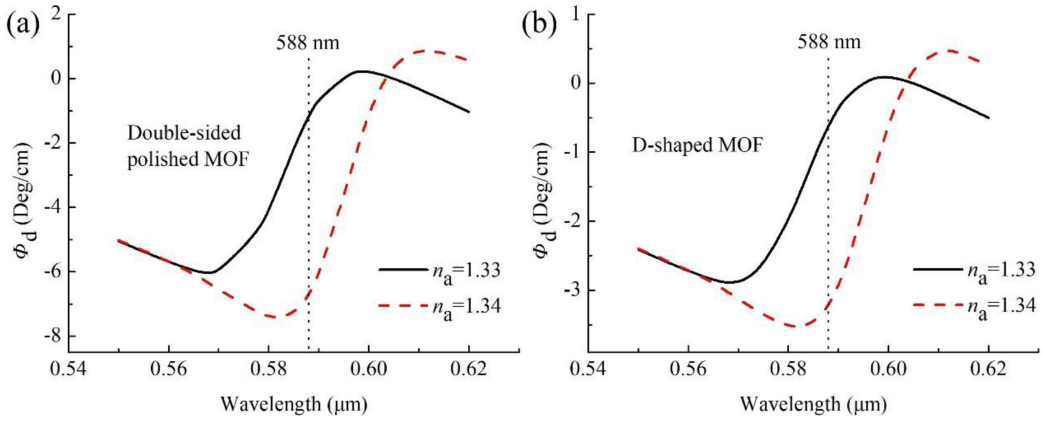

Fig. 5. (a) Phase difference of two modes for the SPR sensor based on double-sided polished MOF with n_a at 1.33 and 1.34. (b) Phase difference of two modes for the SPR sensor based on D-shaped MOF with n_a at 1.33 and 1.34.

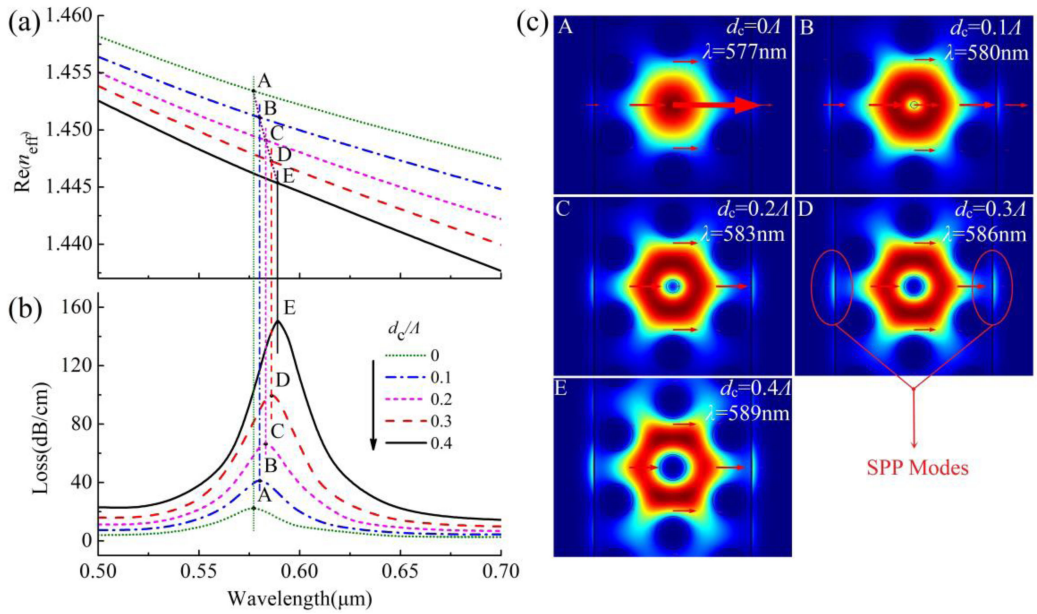

Fig. 6. (a) Re(n_{eff}) curves and (b) loss spectra of the *x*-polarized core mode of the double-sided polished MOF-SPR sensor when d_c/Λ varies from 0 to 0.4. (c) Electric field distributions of the *x*-polarized core mode at the resonance wavelength (phase matching point) with $d_c = 0\Lambda$, 0.1Λ, 0.2Λ, 0.3Λ, 0.4Λ.

where the $\alpha(\lambda, n_a)$ is the propagation loss of *x*-polarized core mode associated with wavelength (λ) and the n_a. L is the length of the sensor, supposing $L = 1/\alpha(\lambda, n_a)$ reasonably [34]. Fig. 4 presents the amplitude sensitivity (S_A) curves of the two structures at n_a varying from 1.33 to 1.34. The maximum S_A of the double-sided MOF-SPR sensor and the D-shaped MOF-SPR sensor are 129.21 RIU^{-1} at 604 nm and 128.99 RIU^{-1} at 605 nm, respectively. Thus it can be verified that the two sensors have almost the same maximum S_A. One difference here, however, is that a short sensor length (L) in the double-sided structure is required to achieve maximum S_A due to its higher mode loss $\alpha(\lambda, n_a)$.

C. Phase Interrogation Mode

The phase interrogation mode, deriving from the phase difference, is special property of the D-shaped SPR sensor in which the incident light is split into two orthogonally polarized components, one of which does not resonate with the SPP mode [40], [41]. The change of the phase difference of the *x*-polarized core mode and *y*-polarized core mode can judge the change in n_a. The phase difference Φ_d can be expressed as [40], [41]

$$\Phi_d = \frac{2\pi}{\lambda} \left(\mathrm{Re}\left(n_p\right) - \mathrm{Re}\left(n_s\right) \right) L \tag{5}$$

where L is the length of sensor, Re(n_p) and Re(n_s) represent the real part of effective index of *x*-polarized core mode and *y*-polarized core mode, respectively.

Fig. 5 shows the Φ_d of double-sided polished and D-shaped MOF-SPR sensors with the n_a changing from 1.33 to 1.34, respectively. The maximum change for Φ_d of the double-sided polished design is 5.53 Deg/cm at 588 nm, while that of the D-shaped design is 2.61 Deg/cm at 588 nm, which means the maximum phase sensitivity of the double-sided polished design is 553 Deg/RIU/cm, nearly twice as much as that of the D-shaped design. Compared with the D-shaped design, the double-sided

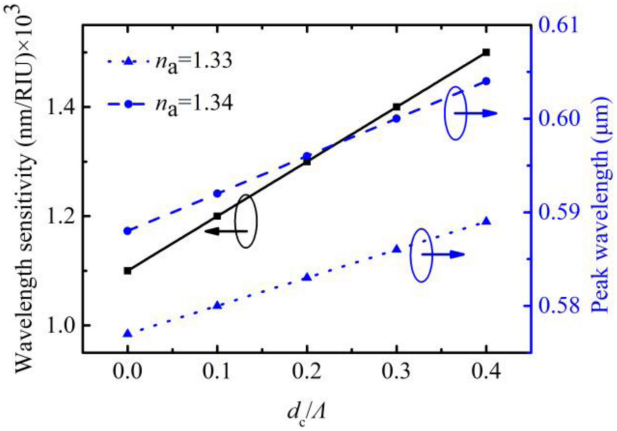

Fig. 7. Wavelength sensitivities and peak wavelengths of x-polarized core mode of the double-sided polished MOF-SPR sensor for different d_c when n_a from 1.33 to 1.34.

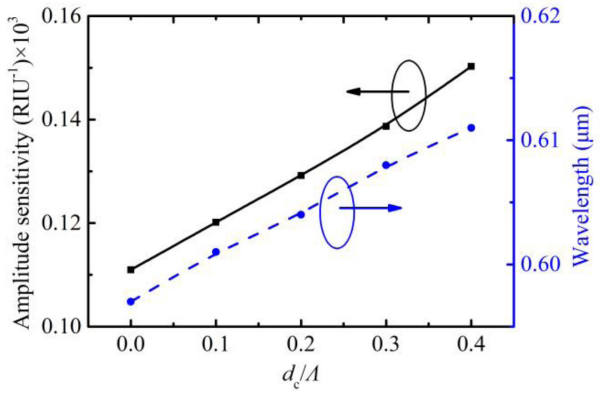

Fig. 8. Maximum amplitude sensitivities and operation wavelengths of x-polarized core mode of the double-sided polished MOF-SPR sensor for various d_c.

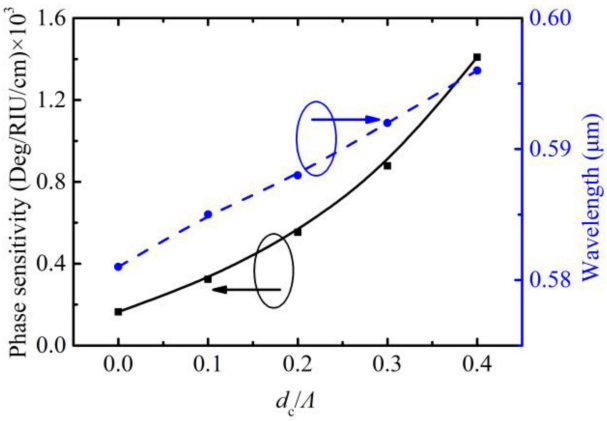

Fig. 9. Maximum phase sensitivities and operation wavelengths of the double-sided polished MOF-SPR sensor for various d_c.

polished design not only improves the intensity of the resonance between the core mode and the SPP mode, but also enhances the birefringence of the core modes which mainly contribute to the phase sensitivity [40], [41].

IV. Discussion

A. *Influence of the d_c on Sensing Performance*

The sensing performance of the sensors can be readily tuned by varying MOF structural parameters, particularly the air hole in the core area [34]–[39]. In what follows, we will study and discuss the d_c on the sensing performance of the proposed sensor, including the SPR spectra, wavelength sensitivities, amplitude sensitivities and phase sensitivities.

In the condition of the above setting parameters, the real part of n_{eff} (Re(n_{eff})) of core mode and loss spectra of the x-polarized core mode for various d_c are numerically simulated and plotted in Fig. 6(a) and (b) by different colors and types of curves. The perpendicular line denotes the wavelength of the corresponding resonance wavelength (phase matching point). As d_c increasing from 0 to 0.4Λ, Re(n_{eff}) of x-polarized core mode shows the decreasing trend obviously, as depicted in Fig. 6(a), resulting in the phase matching point between the x-polarized core mode and SPP mode moving to the longer wavelength. It is much easier observed that the larger hole in the fiber core is, the more electric field adjacent to metallic surfaces leak out, and accompanying with more energy coupling to SPP mode at the resonance wavelength, as shown in Fig. 6(c).

The peak wavelength at $n_a = 1.33$ and 1.34 and wavelength sensitivities of x-polarized core mode for d_c variation are plotted in Fig. 7, where peak wavelength exhibits a tendency of linear growth proportional to d_c/Λ and S_λ corresponding also increases. An increase in d_c/Λ contributes to a decrease in Re(n_{eff}) of core mode, and thus leading to the shift of resonance wavelength to the right, which further promotes notably the ability in penetration for plasmon, and thus enhancing the wavelength sensitivity.

Fig. 8 presents the maximum S_A and operation wavelengths of x-polarized core mode of the double-sided polished MOF-SPR sensor for various d_c. As shown in Fig. 8, The black solid line represents the maximum S_A and the blue dotted line represents the operation wavelength corresponding to maximum S_A, both of which increase as d_c increasing. For example, when d_c is 0.1Λ, maximum S_A is 120.15 RIU^{-1} at $\lambda = 601$ nm. While maximum S_A is obtained at $d_c = 0.4\Lambda$ and $\lambda = 611$ nm, with a value of 150.27 RIU^{-1}. The distinct increase in maximum S_A is due to the fact that increasing d_c increases the $\Delta\lambda_{\text{peak}}$ when the n_a changes from 1.33 to 1.34, and leading to a higher $\Delta\alpha(\lambda, n_a)$ in (4). Furthermore, the maximum $\Delta\alpha(\lambda, n_a)$ always occurs in the vicinity of the peak wavelength, and therefore the operation wavelength of the maximum S_A also increases as the d_c increasing.

The maximum phase sensitivities and operation wavelengths of the double-sided polished MOF-SPR sensor with d_c variation are described in Fig. 9, which implies that with d_c increment the phase sensitivity and operation wavelength are both growing gradually. For instance, with $d_c = 0.4\Lambda$, the maximum phase sensitivity can reach 1408.81 Deg/RIU/cm at 596 nm, which is far more than that of 323.69 Deg/RIU/cm at 585 nm with $d_c = 0.1\Lambda$. The increase of d_c plays a facilitating role in birefringence of the core modes, causing augment of the Φ_d, as in (5), and thus the maximum phase sensitivity (change in Φ_d) is enhanced accordingly. The max change in Φ_d also takes place near the

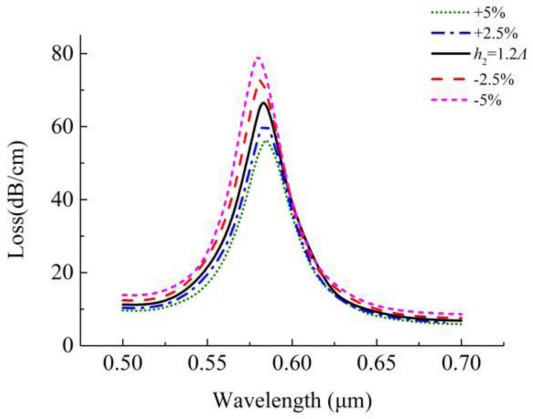

Fig. 10. Loss spectra of the x-polarized core modes of the double-sided polished MOF-SPR sensor with the variation of $\pm 5\%$ of the polishing depth (h_2) the at $n_a = 1.33$.

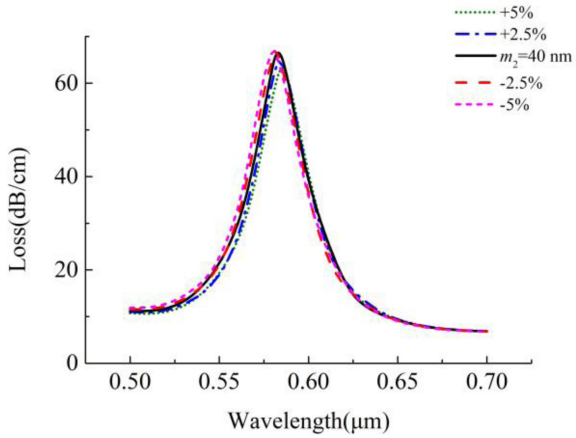

Fig. 11. Loss spectra of the x-polarized core mode with the variation of $\pm 5\%$ of thickness of the gold film (m_2) at $n_a = 1.33$.

peak wavelength, which allows the operation wavelength of the maximum phase sensitivity to increase as well.

Generally, the air hole introduced into the fiber core can improve phase matching between the core modes and the SPP modes efficiently [34]–[39]. By increasing the size of the air hole (d_c), the sensitivities of the sensor, including the wavelength, amplitude and phase sensitivities, can be improved. With the d_c incremental, the maximum phase sensitivity grows faster than the wavelength and amplitude sensitivities which are basically linear increase. Therefore, the increasing d_c is more efficient for maximum phase sensitivity improvement.

B. Influence of Fabrication Tolerance of the h_2 and m_2 on Sensing Performance

For the actual fabricating process, it is difficult to process the symmetrical structure, such as polishing the double sides or depositing the gold film on the two sides in the same parameters. The slight errors in the polishing depths and the gold film thicknesses would disrupt the symmetry of the sensor, and thus affecting the sensor performance. Owing to its symmetrical structure, in this section, we only consider the influence of the fabrication tolerances of h_2 and m_2 in the range of $\pm 5\%$ on sensitivity properties.

The influence of the variation of $\pm 5\%$ of h_2 on the loss spectra of the x-polarized core mode of the double-sided polished MOF-SPR sensor at $n_a = 1.33$ is shown in Fig. 10. It can be seen that as the h_2 increasing, the resonance peak moves to longer wavelength and its loss decreases gradually. This scenario is easy to understand by noting that the increasing h_2 extends the path distance between the core mode and SPP mode, therefore needing longer wavelength to achieve the mode coupling and also weakening the intensity of the mode coupling, and resulting in longer wavelength and lower mode loss of the resonance peak. Note that the spectral width of the resonance peak is narrowest at the $h_2 = 1.2\Lambda$ (the case of symmetric structure), increasing or decreasing h_2 will broaden spectral width.

A comparison of sensitivities with variation of $\pm 5\%$ of h_2 are summarized more roundly in the Table I. For the wavelength interrogation mode, the wavelength sensitivity increases with the h_2 increasing. It can be seen from Table I that the resonance peak shifts to longer wavelength with h_2 increasing, and this shift increases for the same h_2 change at $n_a = 1.34$, which lead to a higher wavelength sensitivity for a larger h_2. For the amplitude interrogation mode, the maximum amplitude sensitivities appear near the $h_2 = 1.2\Lambda$ which is the symmetric structure that excites the resonance peak with the narrowest spectral width. According to the (4), the narrowest spectral width mainly contributes the biggest $\Delta\alpha(\lambda, n_a)$, and thus supporting the maximum amplitude sensitivity. For the phase interrogation mode, the maximum phase sensitivity decreases with the h_2 increasing. This phenomenon is easy to rationalize by noting that the h_2 increases the birefringence of the core modes, which also promotes the phase sensitivity according to the (5). It is worthy to note that, similar to the peak behavior, the operation wavelengths of the maximum amplitude and phase sensitivities also move to longer wavelength as the h_2 increasing. This is because the main factors (the $\Delta\alpha(\lambda, n_a)$ and the birefringence) always achieve extrema in the vicinity of the peak wavelength, which influences the amplitude and phase sensitivities respectively.

The loss spectra of the proposed sensor varied by the variation of $\pm 5\%$ of m_2 at $n_a = 1.33$ are presented in Fig. 11. The resonance peak shifts to longer wavelength while the peak loss decreases gradually with m_2 increasing, which is consistent with that of the other MOF-SPR sensors with the metal film thickness increasing [34]–[38]. This phenomenon also results from the fact that the extended path distance between the core mode and SPP mode, which requires longer wavelength to achieve the mode coupling and while weakens its intensity, and leading to a longer resonance wavelength and a lower peak loss of the peak. It is worthy to note that the spectral width of the resonance peak is also narrowest when the sensor structure is symmetric ($m_2 = 40$ nm).

Table II compares the sensing performance of the proposed SPR sensor with variation of $\pm 5\%$ of m_2 at n_a changing from 1.33 to 1.34 in terms of wavelength interrogation mode, amplitude interrogation mode and phase interrogation mode. In

TABLE I
SUMMARY OF SENSING PERFORMANCE OF THE PROPOSED SENSOR IN VARIATION OF $\pm 5\%$ OF H_2

h_2	Wavelength Interrogation			Amplitude Interrogation		Phase Interrogation	
	Peak Wavelength (nm)		Wavelength Sensitivity (nm/RIU)	Max Amplitude Sensitivity (RIU^{-1})	Operation Wavelength (nm)	Max Phase Sensitivity (Deg/RIU/cm)	Operation Wavelength (nm)
	n_a=1.33	n_a=1.34					
-5%	580.0	591.9	1190	117.21	602	600	585
-2.5%	581.7	594.1	1240	124.87	603	592	587
1.2Λ	583.1	595.9	1280	129.21	604	553	588
+2.5%	584.1	597.2	1310	130.45	606	503	590
+5%	584.8	598.0	1320	129.73	608	455	590

TABLE II
SUMMARY OF SENSING PERFORMANCE OF THE PROPOSED SENSOR IN VARIATION OF $\pm 5\%$ OF M_2

m_2	Wavelength Interrogation			Amplitude Interrogation		Phase Interrogation	
	Peak Wavelength (nm)		Wavelength Sensitivity (nm/RIU)	Max Amplitude Sensitivity (RIU^{-1})	Operation Wavelength (nm)	Max Phase Sensitivity (Deg/RIU/cm)	Operation Wavelength (nm)
	n_a=1.33	n_a=1.34					
-5%	580.3	592.8	1250	123.76	603	523	585
-2.5%	581.8	594.4	1260	127.40	603	550	587
40 nm	583.1	595.9	1280	129.21	604	553	588
+2.5%	584.3	597.2	1290	129.23	606	540	590
+5%	585.4	598.5	1310	128.04	608	514	591

the wavelength interrogation mode, the peak shift caused by the m_2 variation at $n_a = 1.34$ is longer than that at $n_a = 1.33$, and thus providing a higher wavelength sensitivity for a thicker m_2. While in the amplitude interrogation mode, the maximum amplitude sensitivity is located at the vicinity of the $m_2 = 40$ nm. The structure of m_2 also can support the narrowest spectral width of the resonance peak, hence supporting maximal $\Delta\alpha(\lambda, n_a)$ in the (4), and resulting in higher amplitude sensitivity. In the phase interrogation mode, the maximum birefringence for the core mode as well as the maximum phase sensitivity are nearby the m_2 at 40 nm, because the m_2 changing does not destroy the structure of the fiber core. Note that the operation wavelengths of the maximum amplitude and phase sensitivities also change accompanied by the peak moving.

V. CONCLUSION

In this paper, we design a novel SPR sensor based on the double-sided polished hollow-core MOF with a pair of parallelly flat channels for RI sensing. A comparison is made with the D-shaped hollow-core MOF-SPR sensor, which indicates that the proposed sensor gives prominence to less spectrum width of the resonance peak due to its double-sided structure, thus can improve SNR for the wavelength interrogation mode and enhance the maximum phase sensitivity for phase interrogation mode. Furthermore, our results demonstrate that the proposed sensor can work normally with the fabrication tolerance of m_2 and h_2 in the range of $\pm 5\%$. The proposed SPR sensor not only possesses all the advantages of D-shaped MOF-SPR sensor, such as real-time sensing in RI, the evasion of the air holes coated with gold film and filled with analyte, but also provides better sensing performances than the D-shaped MOF-SPR sensor, which endows it with greater prospect for sensing applications.

REFERENCES

[1] A. K. Sharma, A. K. Pandey, and B. Kaur, "A review of advancements (2007–2017) in plasmonics-based optical fiber sensors," *Opt. Fiber Technol.*, vol. 43, pp. 20–34, Jul. 2018.
[2] P. Singh, "SPR biosensors: Historical perspectives and current challenges," *Sens. Actuators, B*, vol. 229, pp. 110–130, Jun. 2016.
[3] B. Lee, S. Roh, and J. Park, "Current status of micro- and nano-structured optical fiber sensors," *Opt. Fiber Technol.*, vol. 15, no. 3, pp. 209–221, Jun. 2009.
[4] J. Homola, S. S. Yee, and G. Gauglitz, "Surface plasmon resonance sensors: Review," *Sens. Actuators, B*, vol. 54, no. 1, pp. 3–15, Jan. 1999.
[5] E. Klantsataya, P. Jia, H. Ebendorff-Heidepriem, T. M. Monro, and A. Francois, "Plasmonic fiber optic refractometric sensors: From conventional architectures to recent design trends," *Sensors*, vol. 17, no. 1, Jan. 2017, Art. no. 12.
[6] W. Jing, A. Hunt, N. Tao, F. Zhang, and S. Wang, "Simultaneous quantification of protein binding kinetics in whole cells with surface plasmon resonance imaging and edge deformation tracking," *Membranes*, vol. 10, no. 9, Sep. 2020, Art. no. 247.
[7] S. Zeng, D. Baillargeat, H.-P. Ho, and K.-T. Yong, "Nanomaterials enhanced surface plasmon resonance for biological and chemical sensing applications," *Chem. Soc. Rev.*, vol. 43, no. 10, pp. 3426–3452, Feb. 2014.
[8] L. Qu *et al.*, "Detection of three different estrogens in milk employing SPR sensors based on double signal amplification using graphene," *Food Anal. Method.*, vol. 14, no. 1, pp. 54–65, Jan. 2021.

[9] T. Srivastava and R. Jha, "Black phosphorus: A new platform for gaseous sensing based on surface plasmon resonance," *IEEE Photon. Technol. Lett.*, vol. 30, no. 4, pp. 319–322, Feb. 2018.

[10] T. Srivastava, A. Purkayastha, and R. Jha, "Graphene based surface plasmon resonance gas sensor for terahertz," *Opt. Quant. Electron.*, vol. 48, no. 6, Jun. 2016, Art. no. 334.

[11] K. N. Shushama, M. M. Rana, R. Inum, and M. B. Hossain, "Graphene coated fiber optic surface plasmon resonance biosensor for the DNA hybridization detection: Simulation analysis," *Opt. Commun.*, vol. 383, pp. 186–190, Jan. 2017.

[12] E. Siyu, Y.-N. Zhang, B. Han, W. Zheng, Q.-L. Wu, and H.-K. Zheng, "Two-channel surface plasmon resonance sensor for simultaneous measurement of seawater salinity and temperature," *IEEE Trans. Instrum. Meas.*, vol. 69, no. 9, pp. 7191–7199, Sep. 2020.

[13] Q.-H. Phan, Y.-R. Lai, W.-Z. Xiao, T.-T.-H. Pham, and C.-H. Lien, "Surface plasmon resonance prism coupler for enhanced circular birefringence sensing and application to non-invasive glucose detection," *Opt. Exp.*, vol. 28, no. 17, pp. 24889–24899, Aug. 2020.

[14] N. Polley, S. Basak, R. Hass, and C. Pacholski, "Fiber optic plasmonic sensors: Providing sensitive biosensor platforms with minimal lab equipment," *Biosens. Bioelectron.*, vol. 132, pp. 368–374, May. 2019.

[15] J. Lao *et al.*, "Gold nanoparticle-functionalized surface plasmon resonance optical fiber biosensor: In situ detection of thrombin with 1 n·M detection limit," *J. Lightw. Technol.*, vol. 37, no. 11, pp. 2748–2755, Jun. 2019.

[16] V. Semwal and B. D. Gupta, "Highly selective SPR based fiber optic sensor for the detection of hydrogen peroxide," *Sens. Actuators, B*, vol. 329, Feb. 2021, Art. no. 129062.

[17] H. Yu, Y. Chong, P. Zhang, J. Ma, and D. Li, "A D-shaped fiber SPR sensor with a composite nanostructure of Mos_2-graphene for glucose detection," *Talanta*, vol. 219, Nov. 2020, Art. no. 121324.

[18] M. Chen, T. Lang, B. Cao, Y. Yu, and C. Shen, "D-type optical fiber immunoglobulin G sensor based on surface plasmon resonance," *Opt Laser Technol*, vol. 131, Nov. 2020, Art. no. 106445.

[19] S. Lee, H. Song, H. Ahn, S. Kim, J.-R. Choi, and K. Kim, "Fiber-optic localized surface plasmon resonance sensors based on nanomaterials," *Sensors*, vol. 21, no. 3, Feb. 2021, Art. no. 819.

[20] Y. Zhao, Z.-Q. Deng, and J. Li, "Photonic crystal fiber based surface plasmon resonance chemical sensors," *Sens. Actuators, B*, vol. 202, pp. 557–567, Oct. 2014.

[21] A. A. Rifat *et al.*, "Surface plasmon resonance photonic crystal fiber biosensor: A practical sensing approach," *IEEE Photon. Technol. Lett.*, vol. 27, no. 15, pp. 1628–1631, Aug. 2015.

[22] E. K. Akowuah, T. Gorman, H. Ademgil, S. Haxha, G. K. Robinson, and J. V. Oliver, "Numerical analysis of a photonic crystal fiber for biosensing applications," *IEEE J. Quantum Electron.*, vol. 48, no. 11, pp. 1403–1410, Nov. 2012.

[23] A. A. Rifat *et al.*, "Photonic crystal fiber based plasmonic sensors," *Sens. Actuators, B*, vol. 243, pp. 311–325, May. 2017.

[24] J. Wang, L. Pei, L. Wu, J. Wang, Z. Ruan, and J. Zheng, "A polarization-independent SPR sensor based on photonic crystal fiber for low RI detection," *Plasmonics*, vol. 15, no. 2, pp. 327–333, Apr. 2020.

[25] N. Luan and J. Yao, "A hollow-core photonic crystal fiber-based SPR sensor with large detection range," *IEEE Photon. J.*, vol. 9, no. 3, Jun. 2017, Art. no. 6802107.

[26] X. Zhou *et al.*, "High-sensitivity SPR temperature sensor based on hollow-core fiber," *IEEE Trans. Instrum. Meas.*, vol. 69, no. 10, pp. 8494–8499, Oct. 2020.

[27] M. Hautakorpi, M. Mattinen, and H. Ludvigsen, "Surface-plasmon-resonance sensor based on three-hole microstructured optical fiber," *Opt. Exp.,* vol. 16, no. 12, pp. 8427–8432, Jun. 2008.

[28] D. Li, W. Zhang, H. Liu, J. Hu, and G. Zhou, "High sensitivity refractive index sensor based on multicoating photonic crystal fiber with surface plasmon resonance at near-infrared wavelength," *IEEE Photon. J.,* vol. 9, no. 2, Apr. 2017, Art. no. 6801608.

[29] N. Luan and J. Yao, "High refractive index surface plasmon resonance sensor based on a silver wire filled hollow fiber," *IEEE Photon. J.,* vol. 8, no. 1, Feb. 2016, Art. no. 4800709.

[30] J. Liao *et al.*, "Highly sensitive near-infrared surface plasmon resonance (SPR) sensor based on birefringent six-core photonic crystal fiber," *J. Mod. Optic.*, vol. 67, no. 19, pp. 1463–1468, Nov. 2020.

[31] J. N. Dash and R. Jha, "Graphene-based birefringent photonic crystal fiber sensor using surface plasmon resonance," *IEEE Photon. Technol. Lett.*, vol. 26, no. 11, pp. 1092–1095, Nov. 2014.

[32] A. A. Rifat, G. A. Mahdiraji, D. M. Chow, Y. G. Shee, R. Ahmed, and F. R. Adikan, "Photonic crystal fiber-based surface plasmon resonance sensor with selective analyte channels and graphene-silver deposited core," *Sensors*, vol. 15, no. 5, pp. 11499–11510, May. 2015.

[33] Z. Fan *et al.*, "High sensitivity of refractive index sensor based on analyte-filled photonic crystal fiber with surface plasmon resonance," *IEEE Photon. J.,* vol. 7, no. 3, Jun. 2015, Art. no. 4800809.

[34] A. Hassani and M. Skorobogatiy, "Design criteria for microstructured-optical-fiber-based surface-plasmon-resonance sensors," *J. Opt. Soc. Amer. B*, vol. 24, no. 6, pp. 1423–1429, Jun. 2007.

[35] A. Hassani and M. Skorobogatiy, "Design of the microstructured optical fiber-based surface plasmon resonance sensors with enhanced microfluidics," *Opt. Exp.*, vol. 14, no. 24, pp. 11616–11621, Nov. 2006.

[36] B. Gauvreau, A. Hassani, M. F. Fehri, A. Kabashin, and M. Skorobogatiy, "Photonic bandgap fiber-based surface plasmon resonance sensors," *Opt. Exp.*, vol. 15, no. 18, pp. 11413–11426, Sep. 2007.

[37] Y. Zhang *et al.*, "Microstructured fiber based plasmonic index sensor with optimized accuracy and calibration relation in large dynamic range," *Opt. Commun.*, vol. 284, no. 18, pp. 4161–4166, Aug. 2011.

[38] X. Yu *et al.*, "A selectively coated photonic crystal fiber based surface plasmon resonance sensor," *J. Opt.*, vol. 12, no. 1, Jan. 2010, Art. no. 015005.

[39] Y. Peng, J. Hou, Z. Huang, and Q. Lu, "Temperature sensor based on surface plasmon resonance within selectively coated photonic crystal fiber," *Appl. Opt.*, vol. 51, no. 26, pp. 6361–6367, Sep. 2012.

[40] N. Luan, R. Wang, W. Lv, and J. Yao, "Surface plasmon resonance sensor based on D-shaped microstructured optical fiber with hollow core," *Opt. Exp.*, vol. 23, no. 7, pp. 8576–8582, Apr. 2015.

[41] Z. Tan, X. Hao, Y. Shao, Y. Chen, X. Li, and P. Fan, "Phase modulation and structural effects in a D-shaped all-solid photonic crystal fiber surface plasmon resonance sensor," *Opt. Exp.*, vol. 22, no. 12, pp. 15049–15063, Jun. 2014.

[42] C. Liu *et al.*, "Surface plasmon resonance (SPR) infrared sensor based on D-shape photonic crystal fibers with ITO coatings," *Opt. Commun.*, vol. 464, Jun. 2020, Art. no. 125496.

[43] L. Zhao, H. Han, Y. Lian, N. Luan, and J. Liu, "Theoretical analysis of all-solid D-type photonic crystal fiber based plasmonic sensor for refractive index and temperature sensing," *Opt. Fiber Technol.*, vol. 50, pp. 165–171, Jul. 2019.

[44] N. Luan, L. Zhao, Y. Lian, and S. Lou, "A high refractive index plasmonic sensor based on D-shaped photonic crystal fiber with laterally accessible hollow-core," *IEEE Photon. J.*, vol. 10, no. 5, Sep. 2018, Art. no. 6803707.

[45] J. N. Dash and R. Jha, "Highly sensitive side-polished birefringent PCF-based SPR sensor in near iR," *Plasmonics*, vol. 11, no. 6, pp. 1505–1509, Dec. 2016.

[46] J. N. Dash and R. Jha, "Highly sensitive d shaped PCF sensor based on SPR for near iR," *Opt. Quant. Electron.*, vol. 48, no. 2, Feb. 2016, Art. no. 137.

[47] N. Luan, R. Wang, W. Lv, and J. Yao, "Surface plasmon resonance sensor based on exposed-core microstructured optical fibers," *Electron. Lett.*, vol. 51, no. 9, pp. 714–715, Apr. 2015.

[48] N. Luan, H. Han, L. Zhao, J. Liu, and J. Yao, "Opening up dual-core microstructured optical fiber-based plasmonic sensor with large detection range and linear sensitivity," *Opt. Mater. Exp.*, vol. 9, no. 2, pp. 819–825, Feb. 2019.

[49] H. Han *et al.*, "Surface plasmon resonance sensor based on dual-side polished microstructured optical fiber with dual-core," *Sensors*, vol. 20, no. 14, Jul. 2020, Art. no. 3911.

[50] N. Luan and J. Yao, "Surface plasmon resonance sensor based on exposed-core microstructured optical fiber placed with a silver wire," *IEEE Photon. J.,* vol. 8, no. 1, Feb. 2016, Art. no. 4800508.

[51] L. Zhao, H. Han, N. Luan, J. Liu, L. Song, and Y. Hu, "A temperature plasmonic sensor based on a side opening hollow fiber filled with high refractive index sensing medium," *Sensors*, vol. 19, no. 17, Sep. 2019, Art. no. 3730.

[52] N. Luan, C. Ding, and J. Yao, "A refractive index and temperature sensor based on surface plasmon resonance in an exposed-core microstructured optical fiber," *IEEE Photon. J.*, vol. 8, no. 2, pp. 1–8, Apr. 2016.

[53] H. Han *et al.*, "A large detection-range plasmonic sensor based on an H-shaped photonic crystal fiber," *Sensors*, vol. 20, no. 4, Feb. 2020, Art. no. 1009.

[54] A. Vial, A. S. Grimault, D. Macías, D. Barchiesi, and M. L. de la Chapelle, "Improved analytical fit of gold dispersion: Application to the modeling of extinction spectra with a finite-difference time-domain method," *Phys. Rev. B*, vol. 71, no. 8, Feb. 2005, Art. no. 085416.